Machine Learning and Optimization Techniques for Automotive Cyber-Physical Systems: Predictive Control During Acceleration Events to Improve Fuel Economy

Samantha White, Aaron Rabinowitz, Chon Chia Ang, David Trinko, and Thomas Bradley

Abbreviations

Abbreviations

AE	Acceleration Event. 650, 651, 656–658, 661–664, 666
APP	Accelerator Pedal Position. 663, 664
BMS	Battery Management System. 659, 661
BPPS	Brake Pedal Position Sensor. 661
BSFC	Brake Specific Fuel Consumption. 650, 651, 653, 666
CSU	Colorado State University. 664
DP	Dynamic Programming. 649–657, 664, 667
EM	Electric Motor. 650, 659, 661–664, 667
EPA	Environmental Protection Agency. 655, 657
FE	Fuel Economy. 649–651, 653–655, 657, 658, 666, 667
HEV	Hybrid Electric Vehicles. 649–652, 659, 663, 667
HSC	Hybrid Supervisory Controller. 659, 661, 664, 665
HV	High Voltage. 663
ICE	Internal Combustion Engine. 650, 661–664, 666, 667
IPO	Input-Processing-Output. 661
MPG	Miles Per Gallon. 666
NYCC	New York City Cycle. 657–659

S. White · A. Rabinowitz · C. C. Ang · D. Trinko · T. Bradley (✉)
Department of Systems Engineering, Colorado State University, Fort Collins, CO, USA
e-mail: samwhite@rams.colostate.edu; aaron.rabinowitz@colostate.edu; chon.ang@colostate.edu; dtrinko@colostate.edu; thomas.bradley@colostate.edu

V. K. Kukkala, S. Pasricha (eds.), *Machine Learning and Optimization Techniques for Automotive Cyber-Physical Systems*, https://doi.org/10.1007/978-3-031-28016-0_23

OBC	On-Board Charger. 659
OCM	Optimal Control Matrix. 661, 663–665
Optimal EMS	Optimal Energy Management Strategy. 649–652, 654, 655, 657
P3	Parallel-3. 659, 663
PAE	Predictive Acceleration Event. 650, 651, 657, 659, 661, 663, 664, 666, 667
SOC	State of Charge. 653–657, 661, 663, 664

1 Concept

The transportation sector has grown to become the leading contributor to greenhouse gas emissions, accounting for 36% of U.S. carbon emissions in 2021 [33]. Myriad emissions-reduction targets at all levels of government and industry are set to take effect in the coming decades and will require rapid reductions in transportation emissions, and therefore, to transportation fuel consumption. The emissions of vehicles powered by combustion can be reduced in the near term by improving their fuel efficiency, which is typically measured as Fuel Economy (FE). Common examples of technologies used to increase FE include engine sizing, advanced engine control, friction/mass/drag reduction, and powertrain electrification [13]. We focus on a category of controls-based FE improvement technologies, Optimal Energy Management Strategy (Optimal EMS), which can theoretically enable FE improvements of up to 30% for Hybrid Electric Vehicles (HEV) under conditions of ideal prediction and actuation [5].

An Optimal EMS is the application of optimal control to vehicle powertrain operation with the objective of minimizing fuel consumption (equivalently, maximizing FE). Computation of an Optimal EMS leverages predictions of future states of the vehicle, which are made based on information that may be, for example, gathered by sensors on the vehicle, obtained via communications with other vehicles and infrastructure, or learned based on historical driving data. The Optimal EMS technique was first published by Lin et al. [19], who derived the globally optimal control using Dynamic Programming (DP) for a hybrid electric truck. Since then, researchers have investigated stochastically robust strategies [20, 22, 24, 35, 36] as well as fast computation strategies [10, 11, 16, 23, 25] with the goal of progressing this technology toward commercial implementation. The technology has still not been realized commercially using such strategies, due in part to the computational cost of making predictions and calculating optimal control strategies in real time.

We conceive and test a novel method to realize Optimal EMS implementation. Instead of using a *real-time* computed *non-globally-optimal* EMS such as stochastic dynamic programming, equivalent consumption minimization strategy (ECMS), or

a heuristic method, we use DP to compute *globally optimal* EMS *in advance*. In effect, this enables exchanging infeasible processing power requirements for potentially feasible memory requirements, improving the feasibility of commercial implementation. Furthermore, we target the strategy to one category of driving events, those in which the vehicle is accelerating from one speed (often zero) to another, or Acceleration Event (AE). We choose to target AE because they can be simpler to predict than general driving, and because they account for a high fraction of fuel consumption relative to their time durations. Thus, we refer to this strategy as Predictive Acceleration Event (PAE) control.

In this chapter, we summarize several years of research defining and testing the PAE method, which have resulted in a series of publications, theses, and patents [1, 4, 5, 7, 21, 26, 27, 31, 32]. The current section includes a brief summary of the simulation investigations that established the feasibility and potential of the PAE strategy. Details of the process for implementing the PAE strategy in a physical vehicle are described in Sect. 2, and results from physical testing are presented in Sect. 3.

1.1 Optimal EMS Mechanism

HEV achieve higher FE than conventional internal-combustion-engine-only vehicles in part because they enable the Internal Combustion Engine (ICE) to operate at high efficiency more of the time. This can be conveniently visualized using a Brake Specific Fuel Consumption (BSFC) map, which illustrates the ICE fuel consumption efficiency as a function of engine rotation speed and supplied torque (Fig. 1). HEV leverage their multiple degrees of freedom for power sourcing—power can be supplied by the ICE or the Electric Motor (EM)—to adjust the BSFC "operating points" in ways that pure ICE vehicles cannot. With a given power request, the only means available to ICE vehicles for adjusting torque and/or speed of the engine is to change the gear ratio of the transmission. In contrast, HEV enable much more flexibility because the EM can supply the difference, positive or negative, between the power supplied by the ICE and the requested propulsion power. For example, when operating at low powers/speeds, an HEV can avoid operating the engine at low efficiency either by using the EM to supply all the power, or by running the engine at high power and efficiency to supply propulsion power in addition to regeneration power through the EM.

Optimal EMS leverage predictions to further this FE improvement approach. In addition to modifying the BSFC operating points during each instant, an Optimal EMS aims to modify BSFC operating points over time. For the PAE strategy, the time horizon is on the order of tens of seconds (the duration of an AE). If the speed trajectory of the AE is known in advance, it is possible to use an optimization method such as DP to obtain a time series of BSFC operating points that supply the power needed to complete the AE while globally minimizing fuel consumption.

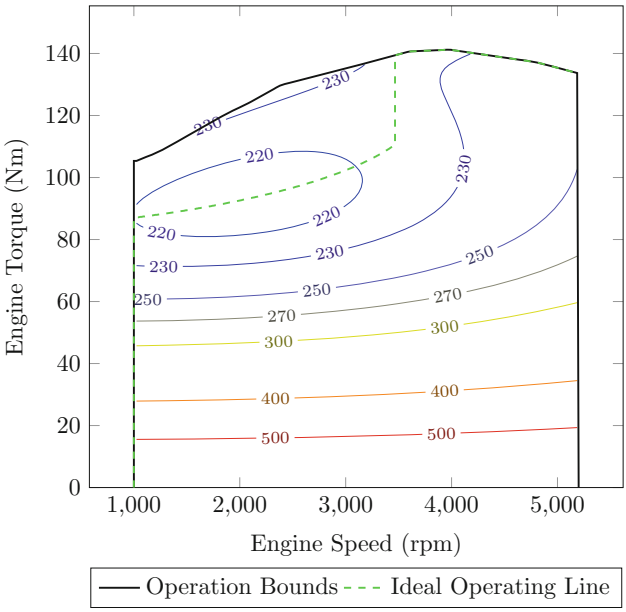

Fig. 1 BSFC map characterizes the fuel efficiency of an internal combustion engine (grams of fuel per kWh supplied) as a function of speed and torque

Table 1 Significant parameters defining the 2010 Toyota prius model

m	1380 kg	A_{front}	2.6005 m^2
$P_{\text{ICE,max}}$	73 kW	C_{rr}	0.008
m_{fuel}	$f(T_{\text{ICE}}, \omega_{\text{ICE}})$[17]	r_{fd}	3.27
$\omega_{\text{trac,max}}$	10,000 rpm	r_{wheel}	0.317 m
$\omega_{\text{gen,max}}$	13,500 rpm	C_d	0.250
$Q_{\text{batt,0}}$	6.5 Ah	V_{oc}	201.6 V
N_{sun}	30	N_{ring}	78
R_{int}	0.373 Ω		

1.2 Model Details

The Toyota Prius has consistently achieved the highest FE in its class [34], so it is an ideal vehicle to model for investigations of new HEV FE improvement techniques. The 2010 model was chosen for its commercial prevalence and publicly available parameter information. A model of the 2010 Toyota Prius, derived using the Autonomie modeling software, has been shown to correlate closely with real-world performance [18]. The referenced model is not publicly available, so a model was developed and validated by modifying a 2004 Toyota Prius model included with Autonomie with 2010 Prius parameters. Table 1 is a list of key parameters defining the model, where m = vehicle mass; $P_{\text{ICE,max}}$ = maximum engine power;

m_{fuel} is the fuel consumption model; T_{ICE} = engine torque; ω_{ICE} = engine speed; $\omega_{\text{trac,max}}$ is the maximum traction motor speed; $\omega_{\text{gen,max}}$ is the maximum generator motor speed; $Q_{\text{batt,0}}$ is the initial battery capacity; N_{sun} and N_{ring} are the number of teeth on the sun and ring gears in the planetary gearset; R_{int} is the battery's internal resistance; A_{front} is the frontal area of the vehicle; C_{rr} = coefficient of rolling resistance; r_{fd} = final drive ratio; r_{wheel} = wheel radius; C_d = drag coefficient; and V_{oc} = open circuit battery potential.

The Autonomie software produces high fidelity models that are useful for realistic modeling of a variety of vehicle signals, including power split control in a HEV, but are computationally expensive in simulation. Even if disregarding concerns about long computation times, it would be infeasible to use the Autonomie model with DP to derive the Optimal EMS, because states in Autonomie are dependent on preceding states, which is incompatible with the DP formulation (described in Sect. 1.2.2). Instead, the Autonomie model was used only to simulate the Baseline EMS engine control strategy, which was used as an input to a lower fidelity "power split" vehicle model for the remaining vehicle signal calculations. Details on the original development of the power split model are in a previous publication from the author's lab group [4] and reproduced briefly here.

The power split model is based on equations describing vehicle dynamics, a modeling approach that is well-defined in the literature [2, 12, 17, 28]. The power required to propel the vehicle at velocity v must be provided as a sum of engine power and electric propulsion system power:

$$P_{\text{prop}} = F_{\text{prop}} v = P_{\text{elec}} + P_{\text{ICE}} \tag{1}$$

P_{ICE} is an input to the power split model, so the equation is rearranged to solve for P_{elec}:

$$P_{\text{elec}} = F_{\text{prop}} v - P_{\text{ICE}} \tag{2}$$

F_{prop} effects vehicle acceleration and counteracts the forces opposing vehicle motion:

$$F_{\text{prop}} = m\dot{v} + C_{rr} mg + \frac{1}{2} C_d \rho_{\text{air}} v^2 A_{\text{front}} \tag{3}$$

where $\dot{v}$ is the acceleration of the vehicle, calculated using a numerical derivative; g is acceleration due to gravity $\left(9.81 \frac{\text{m}}{\text{sec}^2}\right)$; and ρ_{air} is the density of air $\left(1.1985 \frac{\text{kg}}{\text{m}^3}\right)$. For this research, grade angle is assumed to be zero.

P_{elec} is served by the battery, with an efficiency penalty modeled as a function of torque and speed of the generator and traction motors:

$$\eta_{\text{elec}} = f(\omega_{\text{gen}}, T_{\text{gen}}, \omega_{\text{trac}}, T_{\text{trac}}) \tag{4}$$

as defined by efficiency maps supplied with the Autonomie model. η_{elec} is enforced such that energy is always lost due to inefficiencies in the electric system, whether charging or discharging:

$$P_{\text{batt}} = \eta_{\text{elec}} P_{\text{elec}} \text{ if } P_{\text{elec}} \leq 0 \tag{5}$$

$$P_{\text{batt}} = \frac{1}{\eta_{\text{elec}}} P_{\text{elec}} \text{ if } P_{\text{elec}} > 0 \tag{6}$$

where positive values of P_{batt} represent discharging. At timestep i, battery State of Charge (SOC) is calculated for the next timestep $i+1$ using the following equation:

$$\text{SOC}_{i+1} = \text{SOC}_i - \frac{V_{\text{oc}} - \sqrt{V_{\text{oc}}^2 - 4P_{\text{batt}} R_{\text{int}}}}{2R_{\text{int}} Q_{\text{batt,o}}} \Delta t \tag{7}$$

To enable fast computation when solving the DP formulation, fuel consumption is modeled using a cubic response surface [15] representation of a publicly available BSFC map for the Generation III Prius [17]:

$$\begin{aligned} \text{BSFC}\left(\frac{\text{g}}{\text{kWh}}\right) = {} & A_1 + A_2\omega_{\text{ICE}} + A_3 T_{\text{ICE}} + A_4 \omega_{\text{ICE}} T_{\text{ICE}} + A_5 \omega_{\text{ICE}}^2 + \\ & A_6 T_{\text{ICE}}^2 + A_7 \omega_{\text{ICE}} T_{\text{ICE}}^2 + A_8 \omega_{\text{ICE}}^2 T_{\text{ICE}} + A_9 T_{\text{ICE}}^3 \end{aligned} \tag{8}$$

where all A values are fitted constants. This BSFC surface has an ideal operating line [14] that represents the instantaneous optimal FE operating point (in terms of torque and speed) as a function of engine power. The fuel consumption during a timestep Δt is thus

$$m_{\text{fuel}}\,(\text{grams}) = \left(\text{BSFC} \times \frac{1\,\text{h}}{3\,\text{s}}\right) P_{\text{ICE}} \Delta t \tag{9}$$

where P_{ICE} is in kW and Δt is in seconds.

The angular speeds of powertrain components are constrained by a planetary gearset:

$$\omega_{\text{ICE}} = \omega_{\text{gen}} \frac{\rho}{1+\rho} + \omega_{\text{ring}} \frac{1}{1+\rho} \tag{10}$$

where $\rho = \frac{N_{\text{sun}}}{N_{\text{ring}}}$. Speeds are also constrained by limits on the electric motors, given in Table 1. The ring gear speed is linearly related to vehicle speed:

$$\omega_{\text{ring}} = \frac{r_{\text{fd}}}{r_{\text{wheel}}} v \tag{11}$$

The model's powertrain is controlled by one of two different control strategies: a Baseline EMS, meant to simulate stock vehicle performance, and an Optimal EMS, derived via DP to optimize FE over a predicted driving schedule.

1.2.1 Baseline EMS

The Autonomie model is simulated over a drive cycle $v(t)$, defining the Baseline EMS $P_{\mathrm{ICE}}(t)$, which also implicitly defines $P_{\mathrm{elec}}(t)$ via Eq. (2). The power split model is used to calculate the remaining outputs, including m_{fuel}, SOC, and FE. This is illustrated in Fig. 2a.

To validate the Baseline EMS, the process in Fig. 2a was applied to three standard Environmental Protection Agency (EPA) FE test schedules and the FE results, corrected for change in SOC using a method standardized by Society of Automotive Engineers [30], were compared with experimental results for the 2010 Toyota Prius measured by Argonne National Laboratory [3] (Table 2). Additional validation steps included by comparing fuel consumption, SOC, and engine speed traces to actual data. These validations are documented in [31].

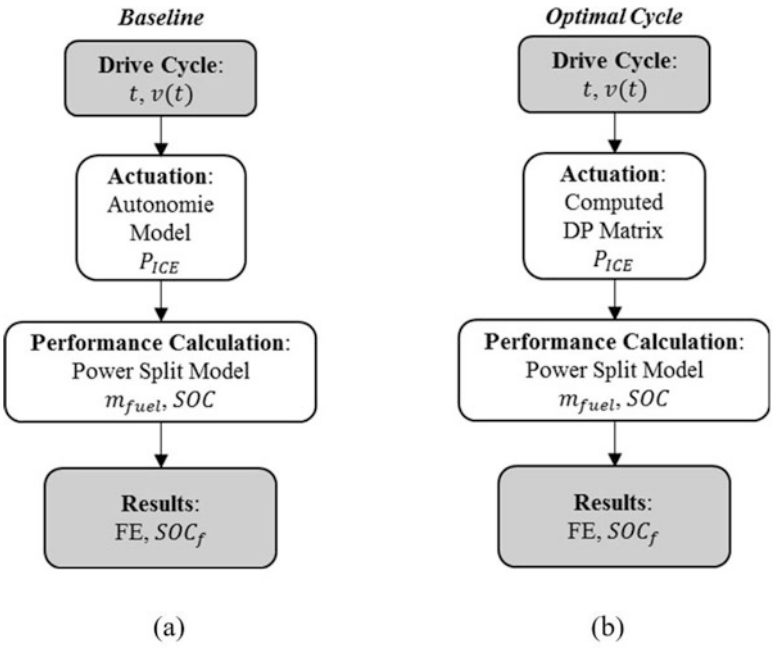

Fig. 2 FE simulation method for (**a**) Baseline EMS and (**b**) Optimal EMS (exact schedule prediction)

Table 2 FE results demonstrating validation of Baseline EMS model for FE investigations

EPA drive cycle	Simulated FE	Measured FE	% Difference
UDDS	76.4 mpg	75.6 mpg	+1.1%
US06	45.0 mpg	45.3 mpg	−0.6%
HWFET	69.1 mpg	69.9 mpg	−1.1%

1.2.2 Optimal EMS

The Optimal EMS is derived using deterministic DP, which uses backwards recursion to avoid solutions that are not optimal as defined by the Bellman Principle of Optimality [8, 9]. The DP scheme used for this study was detailed and validated in a previous publication [4] and will be described only briefly in this section.

In general, DP is used to compute optimal control as a function of system state by minimizing a cost function, subject to system constraints. For this study, the optimal control variable is engine power P_{ICE}, which also implicitly defines P_{elec} via Eq. (2); the state variable is battery SOC; and the cost function is fuel consumption m_{fuel}. For the purposes of the DP scheme, vehicle velocity trace $v(t)$ is an exogenous input upon which the state variable, SOC, partially depends. The state and cost are given by the following equations:

$$\text{SOC}(k+1) = \text{SOC}(k) + f(\text{SOC}, P_{\text{ICE}}, v, k)\Delta t \tag{12}$$

$$\text{Cost} = \sum_{k=0}^{N-1} m_{\text{fuel}} + W\left(\text{SOC}_f - \text{SOC}(N)\right)^2 \tag{13}$$

where W is a penalty weight arbitrarily set at 10,000, k is the timestep index, N is the number of timesteps, and Δt is the size of a timestep. Equation (12) incorporates Eqs. (3)–(7) and (10)–(11), and Eq. (13) incorporates Eqs. (8)–(9). The allowable state and control spaces are

$$40\ \% \leq \text{SOC}(k) \leq 80\ \% \quad (k = 0, \ldots N) \tag{14}$$

$$0\ \text{kW} \leq P_{\text{ICE}}(k) \leq 73\ \text{kW} \quad (k = 0, \ldots N-1) \tag{15}$$

To summarize, the DP scheme is used to calculate engine power (discretization $\Delta P_{ICE} = 0.1$ kW) for every feasible battery SOC (discretization $\Delta\text{SOC} = 0.02\%$) for every timestep in a drive cycle (discretization $\Delta t = 0.4$ s) to minimize fuel consumption for a velocity trace $v(t)$ and desired SOC_f. In future studies, other measurements (e.g. battery temperature) and cost variables (e.g. battery life impacts) may also merit inclusion but were not included in this research.

The output of DP for a velocity trace can be visualized as a two-dimensional matrix of engine power, where row indices represent values of SOC and column indices represent timesteps (see Fig. 3a). For any initial SOC (SOC_i), the DP matrix

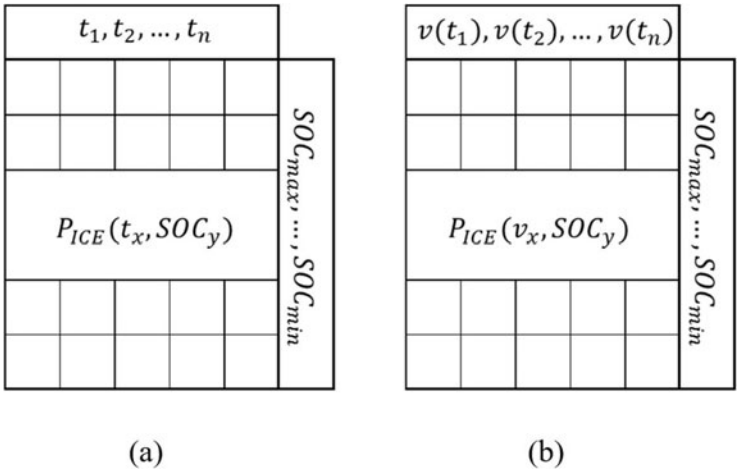

Fig. 3 (**a**) Illustration of matrix generated by dynamic programming algorithm; (**b**) Illustration of matrix with conversion of time index to velocity index

can be used as a lookup table to generate the optimal control solution $P_{\mathrm{ICE}}(t)$ achieving the driving schedule $v(t)$ that results in a desired SOC_f.

1.3 Pre-Computing Optimal EMS for Approximate AE Prediction

Because the matrix generated via DP is a discrete array of optimal $P_{\mathrm{ICE}}(k, \mathrm{SOC})$ for timesteps $k = 0...N$, it can be used as a lookup table for a different drive cycle with the same number of timesteps. This can yield a near-optimal solution if the new drive cycle is similar to the one to which DP was applied. However, the constraint of identical durations makes this method challenging to apply in practice.

If optimal control is only applied to AE, there is a way around the constraint of equal duration. AE are monotonically increasing segments of $v(t)$, so they can be indexed using velocity. This enables the DP matrix to be converted from a mapping with respect to time and SOC ($P_{\mathrm{ICE}}(k, \mathrm{SOC})$) to a mapping with respect to *velocity* and SOC ($P_{\mathrm{ICE}}(v_k, \mathrm{SOC})$), as shown in Fig. 3. With this conversion, it is possible to derive a DP matrix for one AE (the "expected AE") and apply it to any other AE ("actual AE") with the same velocity range as the expected AE, regardless of any difference in duration. Whereas drivers are not necessarily constrained to repeat AE with equal time durations, accelerator pedal traces, or other attributes, traffic laws encourage repetition of AE with equal velocity ranges (for example, 0–25 mph AE on neighborhood streets). Thus, a single DP matrix can serve as a lookup table for improved control of any AE with a similar velocity range to the AE for which it is computed.

In our simulations, a global upper limit to FE during a full drive cycle (containing one or more AE) is achieved by applying DP to compute optimal control for the full velocity profile of a drive cycle, a scenario we refer to as "optimal cycle control." When a DP matrix is computed for an AE and applied to control that same AE, we refer to this implementation as "optimal AE control." (By assuming knowledge of an exact velocity profile, these control scenarios simulate situations in which an AE or a full drive cycle is predicted exactly and DP is applied in real time. Due to sensing, predicting, and computing limitations, we assume these scenarios to be infeasible in practice.) When, instead, a DP matrix is computed for a category of AE (defined by its starting and ending speeds) and applied to another member of that category, this simulates a disturbance to the control loop. Thus, we refer to it as "disturbed AE control."

1.4 Drive Cycle Simulations

A variety of driving schedules, or drive cycles, were simulated to investigate the feasibility of the PAE strategy in real driving contexts. Because city driving is typically characterized by many low-speed AE, the PAE strategy demonstrates highest FE improvement potential when applied to city driving cycles. In this section, we present simulation results for a standard EPA city cycle, the New York City Cycle (NYCC). These simulations demonstrate that FE improvement potential is high for both Optimal Cycle and Optimal AE control, and Disturbed AE FE is nearly as high as Optimal AE FE. Most likely as a result of the low-aggression driving common to these cycles, effective fuel consumption reduction is achieved in the vast majority of AE, leading to high FE gains. The simulated FE results are plotted in Fig. 4 and selected simulation outputs are plotted in Fig. 5.

The Disturbed Optimal EMS achieves a significant portion (77%) of the FE improvement achieved by Optimal AE control and 35% of the FE improvement achieved by Optimal Cycle control. With the exception of some instances of high engine power for SOC correction, the Disturbed engine power trace appears to follow the Optimal AE engine power trace closely, indicating that the categorization scheme sufficiently limits prediction error to provide a close match between the Expected and Actual Optimal EMS.

The FE results for all seven drive cycles simulated, sorted in order of increasing Disturbed AE FE improvement, are given in Fig. 6. The cycle for which Disturbed AE control is least successful is US06, the aggressive cycle; the next three are the highway cycles; and the cycles with the best Disturbed AE performance are the city cycles. This is one indication that Disturbed AE control is most successful in city driving and less successful with increasing aggressiveness.

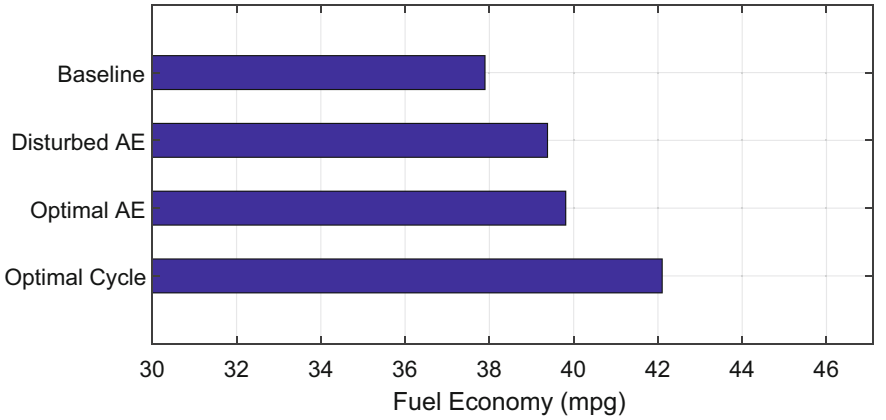

(a)

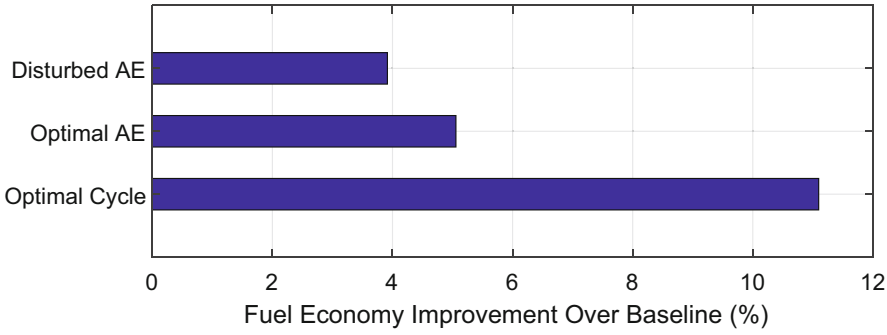

(b)

Fig. 4 FE results for NYCC cycle. (**a**) NYCC cycle FE results. (**b**) NYCC cycle FE improvement results

2 Implementation

In order to physically validate the effectiveness of PAE control, a Parallel-3 (P3) HEV was developed from a stock 2018 Toyota Tacoma [1, 21]. In a P3 HEV, the EM is located in between the transmission and the differential. This vehicle configuration was chosen for a number of reasons. The first was the relative ease of manufacturing in comparison to the other types of hybrid configurations. This type of powertrain was also comparatively easier to implement a supervisory controller in. The P3 configuration allowed the main structure of the vehicle to remain relatively unchanged.

This modification added an electric motor between the transmission and the differential as well as the necessary components to support the electrified powertrain.

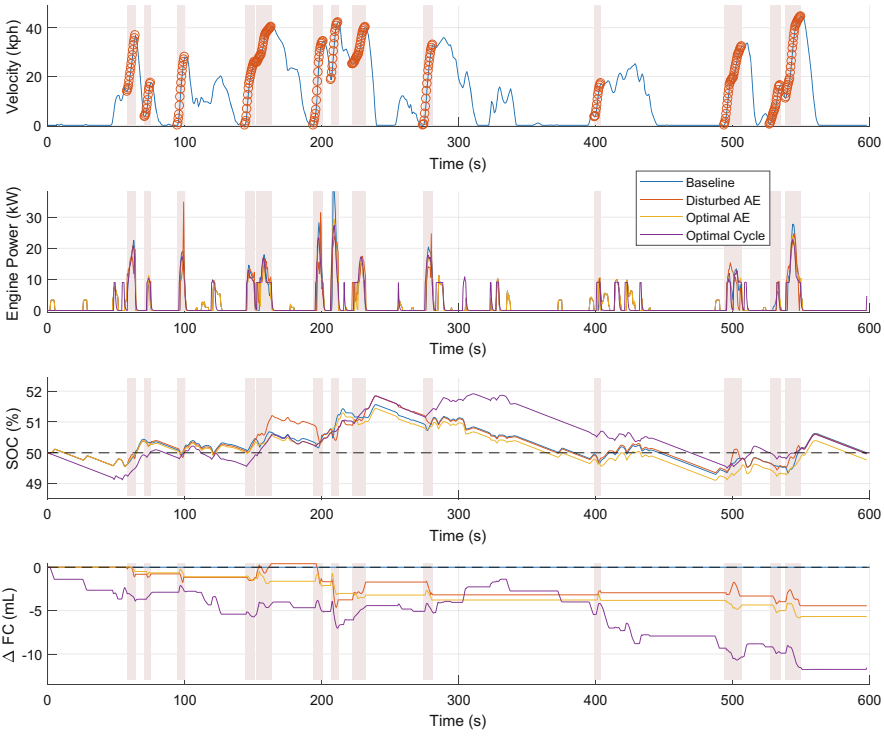

Fig. 5 Simulation outputs for the NYCC cycle

This included the Inverter, Battery, Battery Management System (BMS), Hybrid Supervisory Controller (HSC), Toyota Gateway, On-Board Charger (OBC), and the needed 12 volt powered components to control and provide thermal regulation of the components.

Central to this project was the desire to implement PAE control in a manner which fit industry norms. For this reason, in addition to the P3 conversion, the group elected to accomplish PAE control by leveraging the vehicle's existing distributed computing network and adding minimal computing load to the vehicle. For this reason, the group elected to control the vehicle using only one additional controller, the HSC. The HSC operated as an Input-Processing-Output (IPO) model where it converted input signals to output signals to control the vehicle's behavior. A 112 pin Woodward Motohawk (ECM-5644-112 SECM-112) was used as the hardware for the HSC. This controller is a typical firmware based automotive controller which might be used on a commercial vehicle. Matlab's Simulink software was the development environment for this program allowing for the use of Woodward's Motohawk rapid controller development software. This software was used to build the HSC code that was compatible with the Motohawk hardware. It also allowed for values within the controller to be viewed and calibrated in real time, on the vehicle.

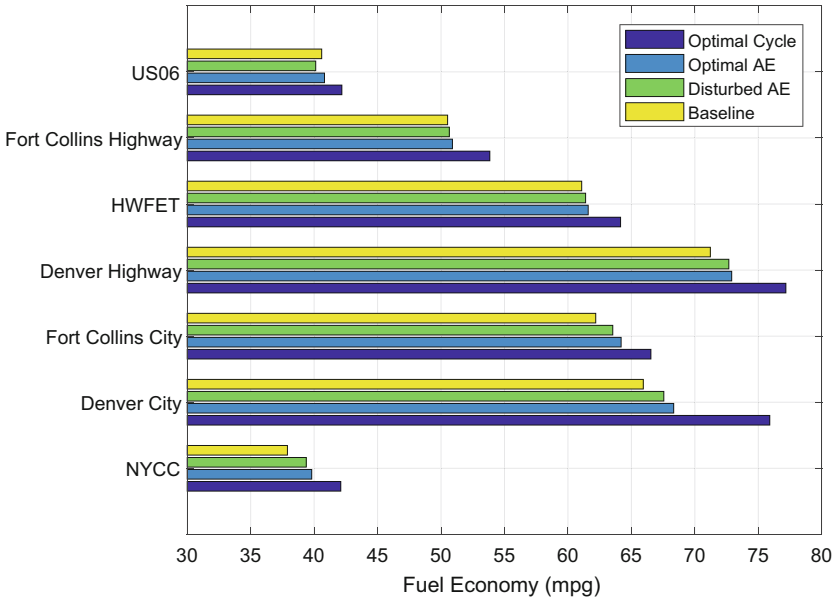

(a)

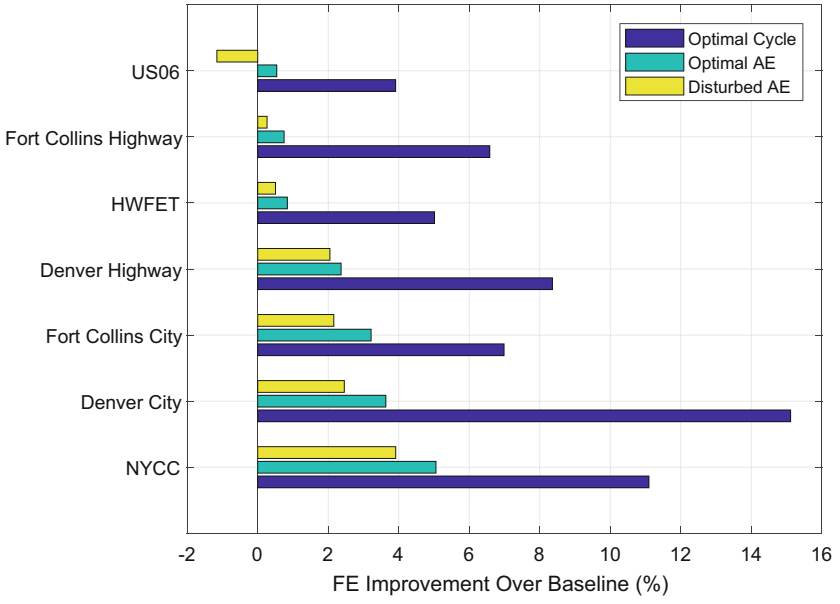

(b)

Fig. 6 FE results for all seven cycles. (**a**) FE for all cycles for all control strategies. (**b**) Improvement over baseline for each control strategy

The selected architecture imposed a series of limitations. When developing the HSC, the following constraints were observed and worked around:

- The HSC's storage capacity was too small to contain a full Optimal Control Matrix (OCM).
- The signals from the Toyota Gateway were the only values that could be used from the base vehicle.
- The BMS was an unreliable source of information, especially with producing SOC values.
- The driver could not consistently reproduce exact AEs under manual control using the accelerator pedal input.
- The HSC had no signal to differentiate between the vehicle's accessory mode and a fully on mode.
- The engine could not be controlled directly by torque requests.
- The Brake Pedal Position Sensor (BPPS) did not output non-binary values.

Figure 7 shows a simplified structure of the HSC and the flow of signals through the controller. It shows the signals that occurred when the vehicle was turned on and off as well as the signals that occurred continuously while the HSC was on. This flowchart illustrates the basic outline of the HSC code. It begins with the input signals and ends with the output signals. The flowchart shows the connection between power mode, vehicle state, pedal logic, torque split, ICE control, inverter and EM control, battery control, and SOC calculations.

With this architecture in mind, a baseline and PAE control were developed.

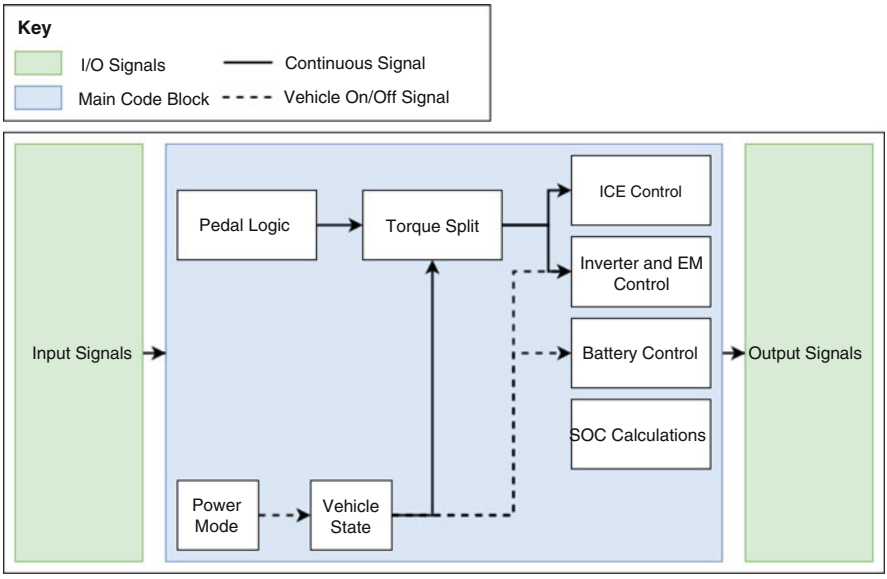

Fig. 7 Simplified controller flowchart

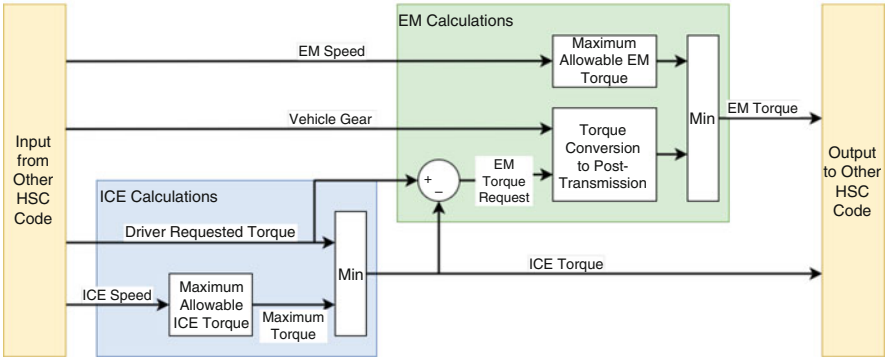

Fig. 8 Baseline torque split

2.1 *Baseline Torque Split Control*

A load following torque split strategy was chosen to act as the Baseline Torque Split Method. The load following method calculated the ICE torque first, compared that torque value to the driver's requested torque, and filled in the difference with EM torque. This method worked in all driving scenarios, and was calculated on the vehicle. No calculations needed to happen before the vehicle was driven. However, this strategy did not provide an optimal torque split for the AE. The flowchart for the Baseline strategy can be found in Fig. 8.

This strategy was composed of two main components: ICE calculations and EM calculations. The ICE calculations started with the minimum of the driver requested torque and maximum allowable torque for the given engine speed being selected for the ICE torque output. The ICE torque output was then subtracted from the driver requested torque to obtain the EM torque request value.

Since this was a P3 HEV, and the ICE and EM were located on opposite sides of the transmission, the EM torque request value must be multiplied by the vehicle gear ratio to obtain the post-transmission EM torque request value. The post-transmission value and maximum allowable EM torque are then compared, with the smaller value selected to be the EM torque output.

2.2 *PAE Torque Split Control*

Two PAE methods were used to calculate torque split values: on-vehicle torque computation through an optimal torque split matrix and pre-computed torque traces. The optimal torque split matrix, used for the on-vehicle torque split computations,

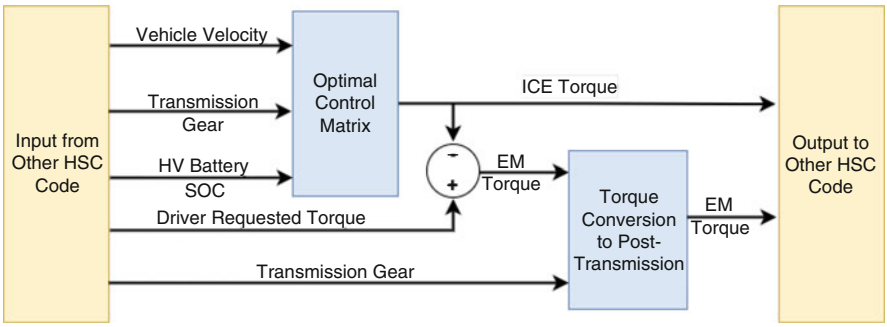

Fig. 9 OCM torque computation flowchart

Fig. 10 Pre-computed torque trace flowchart

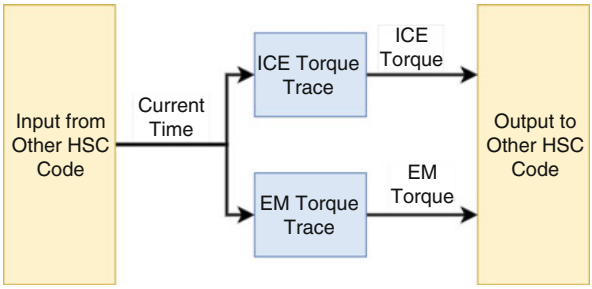

was obtained from the PAE model, as discussed in Sect. 1.3. The pre-computed torque traces were also obtained as an output from this model.

agraphOCM Torque Computation This torque split method required the AEs to be pre-computed to generate an OCM of torque split output values. This OCM was then added to the controller, so that the engine torque could be determined from the SOC and vehicle speed while performing an AE. Figure 9 shows the simplified flowchart of this method.

In this figure, it can be seen that the OCM requires three inputs: vehicle velocity, transmission gear, and the SOC of the High Voltage (HV) battery. This matrix then output the ICE torque which, when subtracted from the driver requested torque, produces the pre-transmission EM torque value. This value then was multiplied by the transmission gear to convert to a post-transmission EM torque value.

agraphPre-Computed Torque Trace The Pre-Computed Torque Trace involved generating the ICE and EM PAE torque traces in advance and using the traces to control the torque instead of the driver's Accelerator Pedal Position (APP) input. Figure 10 shows the flowchart for this PAE method.

As seen in the figure, the current time was input into lookup tables that contained ICE and EM torque traces which converted the time value to a torque output. After each AE, the driver reset the current time value back to zero via a manual switch, located on the vehicle's dashboard. A second dash switch was used to trigger the block that contains the torque trace logic.

3 Results

3.1 PAE Strategy Results

The bulk of the Baseline and PAE comparison testing was completed at the Christman Airfield, a 4000 foot long runway that was used as a Colorado State University (CSU) testing facility. This airfield was used for closed-course, straight-line testing. It runs in a north-south line, and every test that was completed with this vehicle was in the north direction. This reduced the effects of the slight slope of the runway.

The PAE control strategy was tested using the OCM method and the torque trace strategy. The OCM method, reduced in size and scope due to HSC memory limitations, was discovered to output torque split values that didn't prioritize recharging the battery to the starting SOC. Instead, it would command large, positive torque outputs from the EM.

Figure 11 shows one of the tests completed with the OCM generating the torque split between the EM and ICE for the AE. As seen in the figure, the EM torque

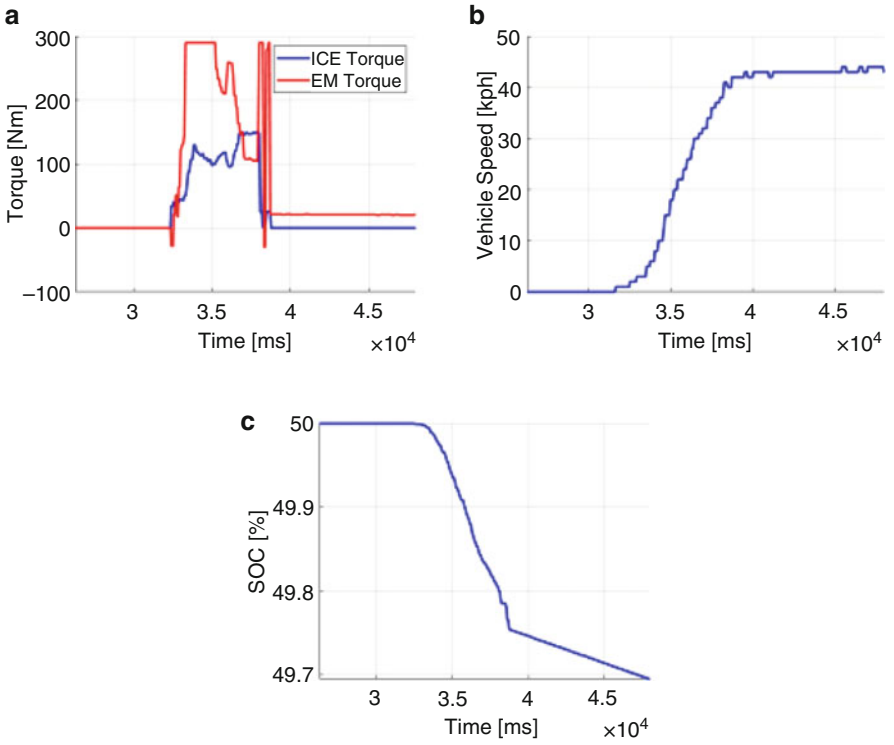

Fig. 11 Results of PAE using OCM method. (**a**) Torque output. (**b**) Vehicle speed trace. (**c**) SOC trace

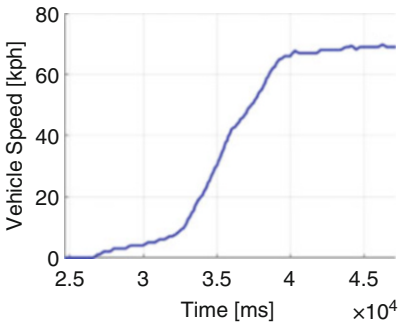

Fig. 12 Vehicle speed trace used to generate pre-computed ICE and EM torque for baseline and PAE method

Table 3 PAE testing results

Mean baseline FE	Mean PAE FE	% Improvement
11.820	16.455	0.282

Table 4 PAE testing results statistics

Number of runs	St.D. of baseline FE	St.D. of PAE FE	Significance (p-value)
5	0.233	0.5267	6.0e-9

was applied at a much larger amount than the ICE torque. If the OCM was working correctly here, the EM torque output would have been negative during the AE to increase the SOC to ensure that the SOC at the beginning and end of the AE were equal. Ultimately, DP based control is subject to discretization and below a certain point, the control will no longer function optimally. The memory limitations on the controller were sufficient to make the matrix method infeasible.

In torque trace method, ICE and EM torque were pre-calculated using the speed trace from Fig. 12. For Baseline, APP signal that would result in the speed trace in Fig. 12 was generated and used as an input to control the vehicle behavior in test. For PAE, ICE and EM torque that would result Fig. 12 was generated and used as an input instead. In contrast, the torque trace method generated more favorable results as the vehicle was to perform as expected when pre-computed torque traces were fed into the HSC. for this reason the torque trace method was selected for data collection.

3.2 PAE vs Baseline Results

PAE control was tested for an AE of 0–30 kph. Results for these events are shown in Tables 3 and 4.

From the tests, it was found that the torque trace PAE method improved the FE by an average of 28.17%. To get to this number, the amount of energy used for the time that it took to complete the AE was converted into a gallon equivalent amount. This was then combined with the fuel usage of the ICE and was used to divide the

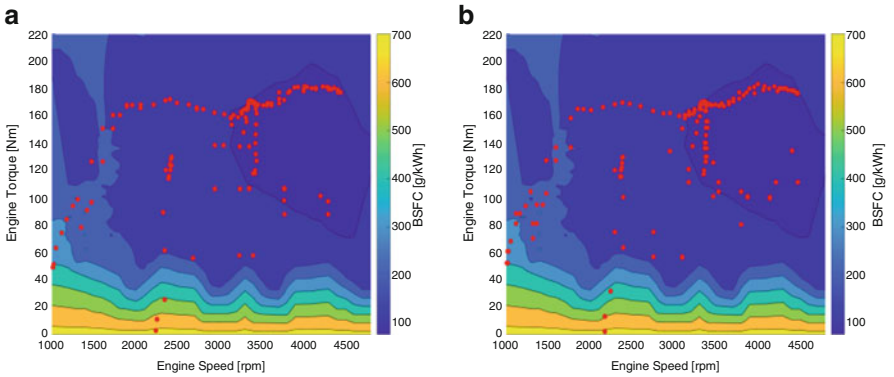

Fig. 13 Engine speed vs engine torque under PAE method. Red dots represent engine behavior during PAE operation. (**a**) PAE AE 1. (**b**) PAE AE 2

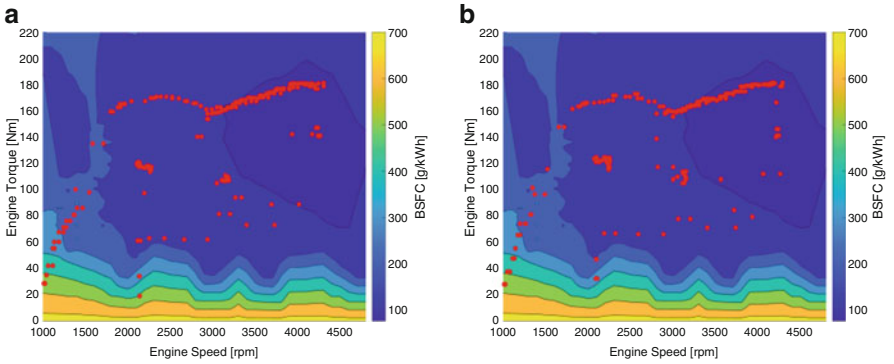

Fig. 14 Engine speed vs engine torque under baseline method. Red dots represent engine behavior during Baseline operation. (**a**) Baseline AE 1. (**b**) Baseline AE 2

distance driven to obtain the Miles Per Gallon (MPG) value. This value could then be used for comparison. For two PAE AEs and two Baseline AEs, the engine torque was plotted against the engine speed on the BSFC map developed previously. This can be seen in Figs. 13 and 14.

The PAE controlled AE shown in Fig. 13a spent 42.9% of the event in the darkest blue, or most fuel efficient zone. Figure 13b shows the next PAE AE which spent 43.7% of the time in that state. Figure 14a's AE, which used Baseline control, spent 29.6% of the event in the dark blue zone. The Baseline controlled AE in Fig. 14b spent 29.1% in the fuel efficient zone. Using this information with the BSFC plots, it can be seen that the AEs using PAE control spend more time with the ICE in the darkest blue, or most fuel efficient, section of the map than the Baseline AEs. The PAE control method was commanding the ICE into the more fuel efficient states during the AE allowing the vehicle to improve the FE by an average of 28.17%.

4 Conclusion

As outlined in Sect. 1, much research has been conducted into the theoretical use of optimal control for torque split in HEVs. Nearly every study of predictive powertrain control to date has used complicated and computationally expensive ways to optimize the operation of the powertrain [6, 29]. These studies include methods like DP, machine learning, and model predictive control to determine the optimal control for the vehicle.

In this study, a map-based control method, based on offline learning was used to realize a pseudo-optimal control that was robust to disturbances and realized measurable fuel economy gain. The control system was able to use the pre-computed PAE values as a lookup table to determine the optimal torque output for the ICE and EM. This meant that by pre-computing the PAE map, the PAE control could occur on the Motohawk control hardware with the rest of the supervisory control algorithm.

Testing this vehicle marked the first time in literature that a test vehicle was able to demonstrate the FE benefits of predictive control algorithms [6]. The previous literature has calculated, modeled, and simulated predictive control hypothesizing the fuel economy benefits while this paper demonstrated the actual improvements in FE for a PAE control when compared to a baseline control.

This real-world validation is significant as, despite research efforts, currently, all of the HEVs on the road currently use instantaneously optimized control to be able to control the powertrain of the vehicle [6]. PAE is an implementable way of improving the FE of HEVs, using information from the predicted vehicle trajectory. This research demonstrated that these strategies were feasible and could improve the FE of HEVs.

References

1. Adelman, D.: Post-transmission parallel hybrid vehicle design and validation for predictive acceleration event energy management strategies. Master's Thesis, Colorado State University, 2021
2. Arata, J.P. III.: Simulation and control strategy development of power-split hybrid-electric vehicles. Ph.D. Thesis, Georgia Institute of Technology, 2011
3. Argonne National Laboratory: Downloadable dynamometer database | argonne national laboratory (2017). https://www.anl.gov/energy-systems/group/downloadable-dynamometer-database, Accessed 16 Oct 2017
4. Asher, Z.D., Baker, D.A., Bradley, T.H.: Prediction error applied to hybrid electric vehicle optimal fuel economy. IEEE Trans. Control Syst. Technol. **26**(6), 1–14 (2017)
5. Asher, Z.D., Trinko, D.A., Bradley, T.H.: Increasing the fuel economy of connected and autonomous Lithium-Ion electrified vehicles. In: Behaviour of Lithium-Ion Batteries in Electric Vehicles. Green Energy and Technology, pp. 129–151. Springer, Cham (2018)
6. Asher, Z.D., Patil, A.A., Wifvat, V.T., et al.: Identification and review of the research gaps preventing a realization of optimal energy management strategies in vehicles. SAE Int. J. Altern. Powertrains **8**(2), 133–150 (2019)

7. Asher, Z.D., Trinko, D.A., Payne, J.D., et al.: Real-time implementation of optimal energy management in hybrid electric vehicles: globally optimal control of acceleration events. J. Dyn. Syst. Meas. Control **142**(8) (2020). https://doi.org/10.1115/1.4046477
8. Bellman, R.: Dynamic programming and lagrange multipliers. Natl. Acad. Sci. **42**(10), 767–769 (1956)
9. Bertsekas, D.P.: Dynamic Programming and Optimal Control, vol. I. Athena Scientific, Nashua (1995)
10. Bianchi, D., Rolando, L., Serrao, L., et al.: A rule-based strategy for a Series/Parallel hybrid electric vehicle: an approach based on dynamic programming. In: ASME 2010 Dynamic Systems and Control Conference. American Society of Mechanical Engineers, pp 507–514 (2010)
11. Borhan, H.A., Vahidi, A., Phillips, A.M., et al.: Predictive energy management of a power-split hybrid electric vehicle. In: 2009 American Control Conference, pp 3970–3976 (2009). ieeexplore.ieee.org
12. Burress, T.A., Campbell, S.L., Coomer, C., et al.: Evaluation of the 2010 toyota prius hybrid synergy drive system (2011). https://doi.org/10.2172/1007833
13. EPA, NHTSA, CARB: Draft technical assessment report: midterm evaluation of Light-Duty vehicle greenhouse gas emission standards and corporate average fuel economy standards for model years 2022-2025 (EPA-420-D-16-900, July 2016). Technical Report, EPA-420-D-16-900, Office of Transportation, Air Quality U.S. Environmental Protection Agency National Highway Traffic Safety Administration U.S. Department of Transportation, and the California Air Resources Board, 2016
14. Frank, A.A.: Control method and apparatus for internal combustion engine electric hybrid vehicles. US Patent 6054844 (2000)
15. Gunst, R.F.: Response surface methodology: process and product optimization using designed experiments. Technometrics **38**(3), 284–286 (1996)
16. HomChaudhuri, B., Vahidi, A., Pisu, P.: Fast model predictive control-based fuel efficient control strategy for a group of connected vehicles in urban road conditions. IEEE Trans. Control Syst. Technol. **25**(2), 760–767 (2017)
17. Kawamoto, N., Naiki, K., Kawai, T., et al.: Development of new 1.8-liter engine for hybrid vehicles. In: SAE Technical Paper. SAE International, 2009. https://doi.org/10.4271/2009-01-1061
18. Kim, N., Rousseau, A., Rask, E.: Autonomie model validation with test data for 2010 toyota prius. In: SAE Technical Paper, SAE International (2012). https://doi.org/10.4271/2012-01-1040
19. Lin, C.C., Kang, J.M., Grizzle, J.W., et al.: Energy management strategy for a parallel hybrid electric truck. In: Proceedings of the 2001 American Control Conference. (Cat. No.01CH37148), vol 4, pp 2878–2883 (2001). ieeexplore.ieee.org
20. Lin, C.C., Peng, H., Grizzle, J.W.: A stochastic control strategy for hybrid electric vehicles. In: Proceedings of the 2004 American Control Conference, vol 5, pp 4710–4715 (2004). ieeexplore.ieee.org
21. Mckenney, B.: Comparison of design and implementation of hybrid systems in prototype vehicles. Master's Thesis, Colorado State University, 2021
22. Onori, S., Serrao, L., Rizzoni, G.: 2010. Adaptive equivalent consumption minimization strategy for hybrid electric vehicles. In: ASME 2010 Dynamic Systems and Control Conference. American Society of Mechanical Engineers, pp. 499–505
23. Onori, S., Serrao, L., Rizzoni, G.: Equivalent consumption minimization strategy. In: Hybrid Electric Vehicles. SpringerBriefs in Electrical and Computer Engineering, pp. 65–77. Springer, London (2016)
24. Opila, D.F., Wang, X., McGee, R., et al.: Real-time implementation and hardware testing of a hybrid vehicle energy management controller based on stochastic dynamic programming. J. Dyn. Syst. Meas Control **135**(2), 021,002 (2013)

25. Paganelli, G., Delprat, S., Guerra, T.M., et al.: Equivalent consumption minimization strategy for parallel hybrid powertrains. In: Vehicular Technology Conference. IEEE 55th Vehicular Technology Conference, VTC Spring 2002 (Cat. No.02CH37367), vol. 4, pp 2076–2081 (2002). ieeexplore.ieee.org
26. Payne, J., Stefanon, H., Geller, B., Aoki, T., Bradley, T., Asher, Z. and Trinko, D.: Colorado State University Research Foundation, Toyota Motor Engineering and Manufacturing North America Inc, 2021. Systems and methods for determining engine start time during predicted acceleration events. U.S. Patent 10,946,852
27. Rabinowitz, A., Araghi, F.M., Gaikwad, T., et al.: Development and evaluation of velocity predictive optimal energy management strategies in intelligent and connected hybrid electric vehicles. Energies **14**(18), 5713 (2021)
28. Rajamani, R.: Vehicle Dynamics and Control. Springer Science & Business Media, New York (2011)
29. Sabri, M., Danapalasingam, K.A., Rahmat, M.F.: A review on hybrid electric vehicles architecture and energy management strategies. Renew. Sust. Energ. Rev. **53**, 1433–1442 (2016)
30. Society of Automotive Engineers: Recommended practice for measuring the exhaust emissions and fuel economy of Hybrid-Electric vehicles. Technical Report, J1711, SAE International, 2002
31. Trinko, D.A.: Predictive energy management strategies for hybrid electric vehicles applied during acceleration events. Master's Thesis, Colorado State University, 2019
32. Trinko, D.A., Asher, Z.D., Bradley, T.H.: Application of pre-computed acceleration event control to improve fuel economy in hybrid electric vehicles. Technical Report, SAE Technical Paper, 2018
33. U.S. Energy Information Administration: Annual Energy Outlook 2022. Technical Report, 2022
34. U.S. Environmental Protection Agency: 2017 best and worst fuel economy vehicles. https://www.fueleconomy.gov/feg/best-worst.shtml, Accessed 16 Oct 2017
35. Vagg, C., Akehurst, S., Brace, C.J., et al.: Stochastic dynamic programming in the Real-World control of hybrid electric vehicles. IEEE Trans. Control Syst. Technol. **24**(3), 853–866 (2016)
36. Yang, C., Du, S., Li, L., et al.: Adaptive real-time optimal energy management strategy based on equivalent factors optimization for plug-in hybrid electric vehicle. Appl. Energy **203**(Supplement C), 883–896 (2017)